AGU PUBLICATIONS

Geophysical Research Letters

RESEARCH LETTER
10.1002/2014GL060618

Key Points:
- Basal topography of melting ice shelves is complex
- Basal terraces appear ubiquitous under melting ice shelves
- Melting concentrates on walls between terraces

Supporting Information:
- Readme
- Movie S1
- Movie S2
- Movie S3

Correspondence to:
P. Dutrieux,
pierre.dutrieux@bas.ac.uk

Citation:
Dutrieux, P., C. Stewart, A. Jenkins, K. W. Nicholls, H. F. J. Corr, E. Rignot, and K. Steffen (2014), Basal terraces on melting ice shelves, *Geophys. Res. Lett.*, *41*, 5506–5513, doi:10.1002/2014GL060618.

Received 24 MAY 2014
Accepted 16 JUL 2014
Accepted article online 21 JUL 2014
Published online 1 AUG 2014

Basal terraces on melting ice shelves

Pierre Dutrieux[1], Craig Stewart[2], Adrian Jenkins[1], Keith W. Nicholls[1], Hugh F. J. Corr[1], Eric Rignot[3,4], and Konrad Steffen[5,6]

[1]British Antarctic Survey, NERC, Cambridge, UK, [2]Scott Polar Research Institute, University of Cambridge, Cambridge, UK, [3]Jet Propulsion Laboratory, Pasadena, California, USA, [4]Department of Earth System Science, University of California, Irvine, California, USA, [5]Swiss Federal Research Institute WLS, Birmensdorf, Switzerland, [6]Institute for Atmosphere and Climate, Swiss Federal Institute of Technology, Zürich, Switzerland

Abstract Ocean waters melt the margins of Antarctic and Greenland glaciers, and individual glaciers' responses and the integrity of their ice shelves are expected to depend on the spatial distribution of melt. The bases of the ice shelves associated with Pine Island Glacier (West Antarctica) and Petermann Glacier (Greenland) have similar geometries, including kilometer-wide, hundreds-of-meter high channels oriented along and across the direction of ice flow. The channels are enhanced by, and constrain, oceanic melt. New meter-scale observations of basal topography reveal peculiar glaciated landscapes. Channel flanks are not smooth, but are instead stepped, with hundreds-of-meters-wide flat terraces separated by 5–50 m high walls. Melting is shown to be modulated by the geometry: constant across each terrace, changing from one terrace to the next, and greatly enhanced on the ~45° inclined walls. Melting is therefore fundamentally heterogeneous and likely associated with stratification in the ice-ocean boundary layer, challenging current models of ice shelf-ocean interactions.

1. Introduction

Oceanic waters above the in situ freezing point melt those faces of marine terminating glaciers and ice shelves with which they come into contact [*Depoorter et al.*, 2013; *Rignot et al.*, 2013]. In West Antarctica and Greenland, where waters reach up to 4 and 8° above freezing, respectively [*Straneo et al.*, 2012; *Whitworth et al.*, 1998], the available oceanic heat is large enough to significantly modify the shape of the ice shelves and the ice front of tidewater glaciers. This in turn impacts the dynamics of ice sheets as the reduction in buttressing allows the outlet glaciers to flow faster into the ocean, increasing their contribution to eustatic sea level rise [*Shepherd et al.*, 2012]. Understanding the spatial distribution of melt and the dynamical coupling operating at the ice-ocean interface is therefore an important step in unraveling the feedback associated with the ocean forcing of ice shelf evolution.

Pine Island Glacier (PIG) in West Antarctica (Figure 1a) and Petermann Glacier (PG) in northwestern Greenland (Figure 1b) are two example systems. PIG has been accelerating [*Joughin et al.*, 2010; *Mouginot et al.*, 2014] up to 4 km yr^{-1} and thinning [*Pritchard et al.*, 2012; *Shepherd et al.*, 2004] over the length of the observational record. It still appears to be in unstable retreat [*Park et al.*, 2013], driven by unpinning from a seabed ridge [*Favier et al.*, 2014] and exposure to variable [*Dutrieux et al.*, 2014; *Jacobs et al.*, 2011; *De Rydt et al.*, 2014] but consistently high ocean temperatures, close to 1°C at the grounding line, where the glacier goes afloat [*Jenkins et al.*, 2010]. Tens of kilometers downstream, water temperatures near the ice/ocean interface remain above freezing [*Stanton et al.*, 2013]. PG velocity, on the contrary, has been relatively stable at just above 1 km yr^{-1} over interannual time scales [*Moon et al.*, 2012; *Rignot and Steffen*, 2008], giving the impression that the glacier is in quasi steady state. Like other glaciers in Greenland, PG is exposed to seasonally varying surface melting in addition to basal melting. Ocean waters reach 0.15°C near the ice shelf grounding line, but further downstream, they are close to freezing [*Johnson et al.*, 2011; *Rignot and Steffen*, 2008]. Finally, PG flows into a fjord that constrains the flow of its ice shelf and that of the underlying water.

Despite these differences, PIG and PG also share similarities. Both have extensive floating ice shelves (Figure 1) that are bathed, at least near their grounding line, in relatively warm waters. Both of their ice shelves display similar geometric features, marked by ocean melt-enhanced [*Dutrieux et al.*, 2013; *Gladish et al.*, 2012; *Rignot and Steffen*, 2008; *Sergienko*, 2013; *Stanton et al.*, 2013] 1–4 km wide, 50–400 m high basal channels. On PG, channels are mainly oriented longitudinally (along the ice flow; Figure 1b). On PIG, longitudinal channels in the center of the fast-flowing ice shelf trunk are flanked by smaller transverse channels (oriented obliquely to the ice flow; Figure 1a).

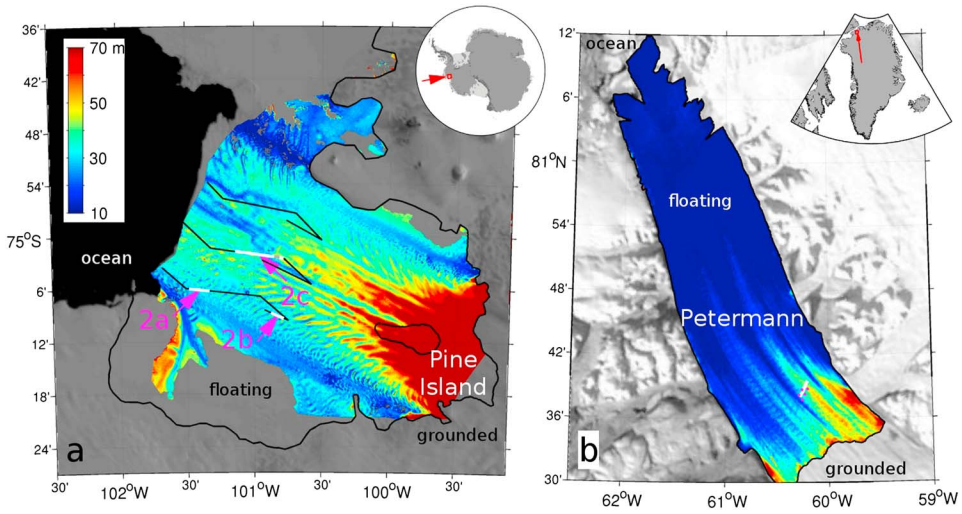

Figure 1. Surface elevation and location of available observations. (a) Surface elevation of Pine Island Glacier ice shelf (color) deduced [*Dutrieux et al.*, 2013] from the SPOT 5 stereoscopic survey of Polar Ice: Reference Images and Topographies project [*Korona et al.*, 2009] overlays a *Moderate Resolution Imaging Spectroradiometer* image obtained on 28 December 2008. The thick black line shows the boundary between floating and grounded ice in 2009 [*Joughin et al.*, 2010]. Autosub tracks with available observations of ice base geometry are displayed by the thin black lines, and the thick white (gray) lines display areas shown in Figures 2a–2c (Figure 2d). The magenta arrows indicate the view direction in Figure 2. (b) Surface elevation of Petermann Glacier ice shelf (color [*Millgate et al.*, 2013]) deduced from the *Advanced Spaceborne Thermal Emission and Reflection Radiometer* satellite in 2006 overlays an image obtained on 19 September 2013 by the Terra satellite. The thick white line (magenta dots) indicates the location of ground-based radar measurements (GPS survey stakes).

This peculiar but generic channel geometry [*Le Brocq et al.*, 2013] fundamentally modifies ice shelf-ocean coupling and dynamics. As a channel is carved by ocean melting, its apex looses hydrostatic support and tends to sag, leading to basal ice divergence [*Jenkins et al.*, 2006] and the formation of a basal crevasse [*Vaughan et al.*, 2012]. This basal signature is accompanied by ice convergence above [*Dutrieux et al.*, 2013; *Jenkins et al.*, 2006], and the formation of surface crevasses on either side. In addition, channel geometry is thought to direct buoyant meltwater plumes and concentrate oceanic melt [*Dutrieux et al.*, 2013; *Stanton et al.*, 2013], potentially allowing ice shelves to survive more ocean heat than they would in the absence of channels [*Gladish et al.*, 2012; *Millgate et al.*, 2013]. Such an apparent paradox between local mechanical weakening and enhanced systemic resilience to oceanic forcing opens new avenues of research in which kilometer-scale ice shelf-ocean interactions are key.

In this paper, we present meter-scale observations of both PIG and PG ice shelf basal geometries and the associated oceanic melting under PG ice shelf. Although derived in two different settings using different technologies, we discuss how the data sets complement each other and shed a new light on the nature of ice-ocean interactions.

2. Data and Methodology

In January 2009, the autonomous underwater vehicle (AUV) Autosub 3 was deployed from the R/V *Nathaniel B. Palmer* under the PIG ice shelf [*Jenkins et al.*, 2010]. During its first three forays beneath the ice shelf (Figure 1a), the AUV was equipped with a Kongsberg EM-2000 multibeam echosounder that was oriented upward to map the underside of the floating ice from a distance of ~100 m. Navigational uncertainty on the swath tracks accumulated at ~1 m in every thousand. Vertical error is on the order of a few centimeters. The ice topography data were processed using the MB System software and gridded using a weighted near-neighbor algorithm. Grids with 2 m cell sizes were used for geomorphic analysis (Figure 2).

In May 2003, on the PG ice shelf, ground-based phase-sensitive radar [*Corr et al.*, 2002] measurements were made along a transect, roughly transverse to the ice flow, ~12 km downstream of PG's grounding line (Figure 1b), allowing a view of the ice shelf basal topography with a 10 m along-track resolution (Figure 3). These observations were complemented by a network of GPS survey stakes surrounding the transect that

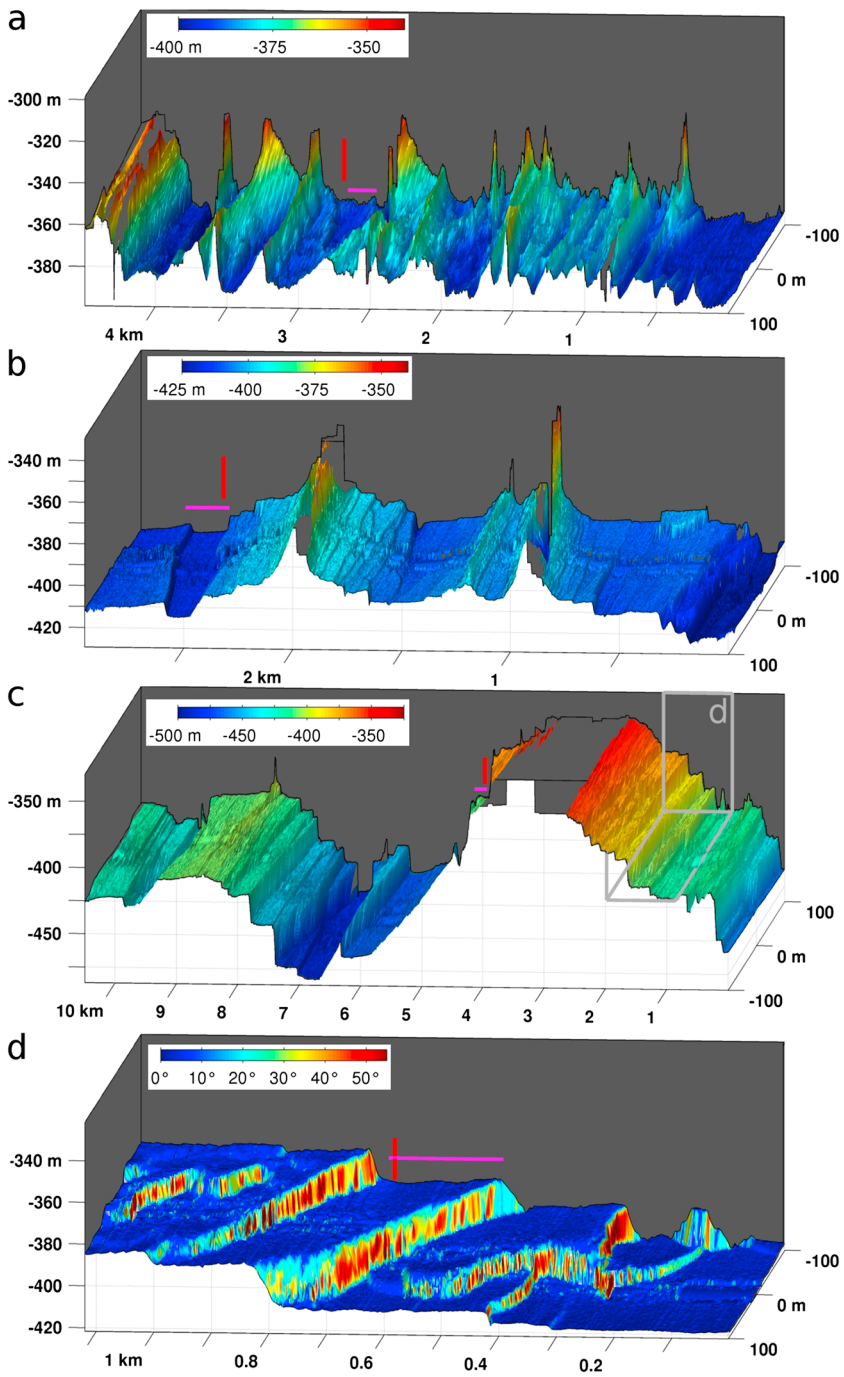

Figure 2. Ice base geometry under Pine Island Glacier ice shelf. (a) Looking upward and sideways, along-track observation of the basal elevation (color) imaged by Autosub near the calving front of Pine Island ice shelf (see Figure 1a for the location and view direction). The red (magenta) lines indicate 20 m (200 m) scale in the vertical (horizontal) direction for reference. (b) Same as in Figure 2a but for transverse channels. (c) Same as in Figure 2a but for longitudinal channels. (d) Basal slope angle from horizontal in the area indicated in Figure 2c.

quantified horizontal surface strain over a 3 day period. Finally, over the course of 1 to 9 days, the same radar observations were repeated 3 to 5 times at selected sites along the transect (gray bars, Figure 3). Following *Jenkins et al.* [2006], we assume no significant change of the ice crystalline structure and basal geometry during those 1 to 9 days. The relative vertical movement of the ice base (black dots, Figure 3a) from an internal reference horizon centered on 35 m depth (henceforth referred to as thinning) is then a result of firn

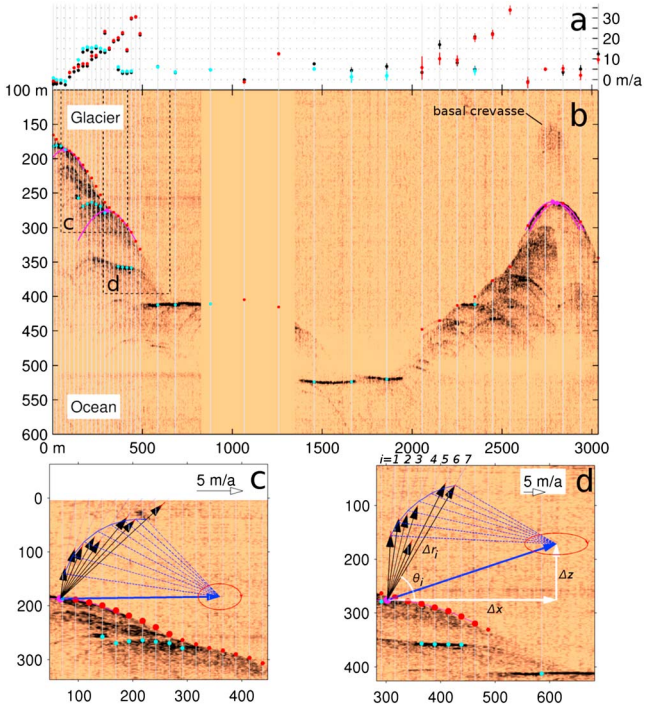

Figure 3. Ice base geometry and melt under Petermann Glacier ice shelf. (a) Along-track estimates of basal melt (color dots) and thinning (black dots) rates at measurement sites (gray lines). The lines indicate 1 standard deviation error bars. (b) Vertical radar amplitude section looking downstream. The positions of first strong radar returns where melt was estimated are displayed by red dots, while the positions of the presumed true basal elevation where melt was estimated are displayed in cyan. Examples of hyperbolas from corner reflectors are shown in magenta. (c–d) Same as in Figure 3b but for enlarging areas with corner reflectors. The black arrows show the melt rate at the corner reflector location (magenta dot) seen from multiple angles (corresponding to large red dot locations). The red lines indicate 1 standard deviation. The blue arrow shows the projected displacement due to melt of the corner reflector obtained by least squares fit. The red ellipse indicates the root-mean-square error of the projected displacement estimate.

compaction, vertical strain in the ice interior as ice converges or diverges horizontally and vertical displacement of the ice/ocean interface due to basal melt. Repeat radar observations taken 1 year apart (in 2002 and 2003) ~3 km upstream of the transverse line indicate that firn compaction effects are negligible (not shown). Vertical strain is deduced from relative movements of internal layers within the upper 200 m of the ice shelf. Melt (colored dots, Figure 3a) is therefore obtained by subtracting strain from thinning. During the survey, vertical strain was a relatively minor component of the overall thinning.

3. Basal Topographies

The geometry of an ice shelf's underside is typically found from airborne radar observations, and their treatment has remained limited in terms of spatial resolution. Even in densely sampled regions on PIG ice shelf, this gave the impression that relatively well resolved, smooth slopes were at times interrupted by poorly resolved basal crevasses [*Vaughan et al.*, 2012]. However, the only available meter-resolution observation of ice shelf basal topography revealed the presence of unevenly spread rugged regions characterized by 20 m elevation changes with similar spatial wavelength [*Nicholls et al.*, 2006]. While airborne radar could misrepresent these features, such ice roughness is likely to affect significantly the nature of the ocean/ice interaction.

Near the southern shear margin of PIG, where both ice deformation and melting are expected to be enhanced by the spatial pattern of subice shelf circulation [*Bindschadler et al.*, 2011; *Jacobs et al.*, 2011], the potentially rugged nature of ice-ocean interface is confirmed under PIG by Autosub observations (Figure 2a), which show a succession of 20–40 m elevation changes with 20 to 100 m spatial wavelengths. If this pattern of irregularly arranged basal grooves extends up to the ice shelf calving front, shallow advection of buoyant meltwater within the groove network could explain apparent discrepancies between the presumed basal depth at the ice front and the depth of a meltwater outflow [*Thurnherr et al.*, 2014].

Away from the ice shelf shear margins, in the central trunk of PIG and PG ice shelves, the ice basal topography is dominated by a coherent arrangement of melt-carved channels. Segments of PIG transverse (Figure 2b) and longitudinal (Figure 2c) channels were imaged by Autosub, confirming their spatial wavelength and amplitude [e.g., *Vaughan et al.*, 2012], as well as revealing with unprecedented spatial resolution the presence of basal crevasses at their apex. Those crevasses are typically 200 m wide at their base, while the airborne radar observations show their height to be typically 200 m [*Vaughan et al.*, 2012].

The channel flanks and keels are not smooth surfaces with typical slopes of 3–5°. Instead, they harbor a succession of hundreds-of-meters-wide nearly horizontal terraces separated by 5–50 m high oblique walls

with typical slopes of 40–60° (Figures 2b–2d). Terrace wall orientation appears complex and intricate (e.g., Figure 2d), and the relatively small area surveyed prevents a significant statistical characterization. A pattern emerges however in which terrace walls are aligned with channel-scale basal topography contours and are generic features not limited to channel flanks (see Movies S1–S3 in the supporting information).

Under PG, lower resolution ground-based radar observations show a very similar basal geometry, with two longitudinal channels of the ice shelf partially imaged by a transverse radar section (Figure 3b). The signature of a ~100 m high basal crevasse can be seen above the only channel apex observed. The keel between channels is unambiguously composed of three terraces 100 to 300 m in width. Channel flank geometry is more difficult to ascertain due to the presence of multiple corner reflectors and their hyperbolic return in radar backscatter amplitudes. First radar returns (red points, Figure 3b) give an impression of relatively smooth slopes. However, strongest radar returns or those that do not fall on hyperbolic shapes (cyan dots) give a rather different perspective, connecting the westernmost channel apex and keel by a succession of terraces and 50–75 m high walls. Consistently, the upper corners of terraces appear to reflect as one-sided hyperbolas in radar returns.

Such terrace geometry therefore seems to be common on the two distinct ice shelves described herein, in different environments, and might be a generic feature of melting ice shelves along with the channels.

4. Associated Ocean Melt

Significant modulation of ocean melt by the basal topography is expected at the channel scale [*Dutrieux et al.*, 2013; *Gladish et al.*, 2012; *Rignot and Steffen*, 2008; *Stanton et al.*, 2013]. Under both PIG and PG's ice shelves, the oceanic thermal forcing is strongest at depth, near the grounding line, which melts the ice and creates a fresh, buoyant plume that rises up the ice base. As the plume gains speed, it entrains more heat from below, renewing that lost to melting, which then increases ocean melting [*Holland et al.*, 2008; *Jenkins*, 1991a]. Given that a buoyant plume rises faster on steeper slopes, enhanced melt is expected to be positively correlated with slope steepness, at least initially. As a channel is being carved and the circulation within it stabilizes, the Coriolis acceleration can play a more significant role.

Initially, melting enhances channels under PIG [*Dutrieux et al.*, 2013]. Under PG, idealized modeling predicts that after enlarging the channels near the grounding line, the flow velocity and adjoining melt are larger on the eastern flanks under the influence of the Coriolis acceleration a few kilometers downstream [*Gladish et al.*, 2012; *Millgate et al.*, 2013]. Ocean physics is likely to be more complex, however, especially in the context of intricate basal topography that potentially modifies ocean circulation, mixing properties, and the relative importance of buoyancy, inertia, and the Coriolis acceleration.

Our estimates of melt on PG are partially consistent with a plume scenario. On the eastern flank of the well-sampled western channel (cyan dots, Figures 3a and 3b), melt increases from near zero near the channel apex to ~15 m yr^{-1} on the channel flank, falling down to ~5 m yr^{-1} at the keel. Melt is therefore strong on the eastern channel flank, but it is also weakest at the top of the channel. Given the expected presence of a relatively cold ~40 m thick mixed layer overlaying warmer waters at the apex of PG's channels [*Rignot and Steffen*, 2008], the available heat there may be insufficient to melt the ice significantly. Near channel keels, it is probably the horizontal flow velocity reduction that lowers the melt rate.

Another observation is that melting magnitude remains relatively constant over terrace flats and jumps from one terrace to the next. Such spatial coherency between geometry and melting confirms that the strongest radar returns (cyan dots, Figure 3) indeed represent basal topography and strongly suggest that other significant returns (e.g., red dots, Figure 3) characterize echoes from side reflectors. It also gives clues about the fundamental role played by the terrace geometry in modulating ice-ocean interactions.

If we assume a hyperbola results from a unique feature (a corner in this case), by observing how the hyperbola (magenta line sampled at the red dots, Figures 3c and 3d) changes over the 1–9 days interval, it is possible to calculate the horizontal and vertical components of motion of the reflecting point. Basically, we assign the displacement measured at each point i of the hyperbola, Δr_i, to a projected displacement of the top of the hyperbola (or corner) in the plane of the radar transect (Figure 3d). If θ_i is the angle from horizontal of the segment joining the reflective corner and the observational station i at the surface of the ice, and $(\Delta x,\Delta z)$ is the true displacement vector of this corner, then the observed projected horizontal displacement is $\Delta r_i = (\Delta x,\Delta z)$.

$(\cos\theta_i, \sin\theta_i) + (\varepsilon_x, \varepsilon_z)$, where $(\varepsilon_x, \varepsilon_z)$ account for misfits. Using available distinct view angles ($i = 1,2,\ldots$), we solve for $(\Delta x, \Delta z)$ and $(\varepsilon_x, \varepsilon_z)$ by least squares fit. Sufficient data are available to do this for two hyperbolas (Figures 3c and 3d), which show that the associated corners move more rapidly horizontally than vertically. Following weak vertical melt at the channel apex, the shallowest observed corner moves mainly eastward at $17 \pm 2\,\mathrm{m\,yr^{-1}}$ (Figure 3c). At the channel flank, a deeper corner moves upward at $13 \pm 3\,\mathrm{m\,yr^{-1}}$ (essentially following the upward movement of the adjacent terrace) but eastward at $39 \pm 7\,\mathrm{m\,yr^{-1}}$ (Figure 3d).

Channelized basal melting causes bending, inducing surface compression, and basal extension over channel apexes. The resulting deformation will produce a relative motion between the surface radar and the basal reflector. The GPS network consistently shows surface divergence of $0.003\,\mathrm{yr^{-1}}$ above the observed channel keel and convergence of $0.003\,\mathrm{yr^{-1}}$ above the eastern channel flank. Assuming that all of this strain is associated with bending, this would give relative motion of ~1 $\mathrm{m\,yr^{-1}}$ for a radar viewing a reflector from a horizontal range of 175 m.

The observed horizontal movement of the corner reflection is an order of magnitude higher and therefore must be induced by melt. This implies that ocean-ice melting processes vary significantly at fine meter scales.

5. Discussion

Ice terraces are sometimes present at the surface of glaciers. In some instances, they are thought to result from mechanical faulting as ice undergoes sudden dynamic instabilities [*De Angelis and Skvarca*, 2003; *Post and LaChapelle*, 1999]. In others, erosional processes are thought to play a major role [*Mölg*, 2003]. In the case of ice shelf basal terraces, our limited observations do not allow us to favor one process for their genesis.

Basal crevasses at channel apexes indicate that significant stresses exist, and the similarity between terrace spatial scales and the ice thickness may point to purely mechanical origins. However, we have not been able to identify breaks in the continuity of faint internal layers that would support the hypothesis of a fracture.

Along with other erosional processes, melting can also be organized by convective oceanic cells and create similar ice geometries in relatively quiescent, vertically stable, stratified laboratory environments [*Huppert and Turner*, 1978]. In colder oceanic settings, stable step-like thermohaline ocean structures with vertical scales similar to those we observe have previously been thought to result from such organized melting [*Jacobs et al.*, 1981]. In the dynamic setting of PIG and PG, the presence of steady convective cells and associated thermohaline staircases appears unlikely and has not been observed yet [*Stanton et al.*, 2013].

Finally, like the larger channels in which they are embedded, terraces could result from a complex coupled interaction between the ice and the ocean. Without considering the channel or cavity-scale circulation, and placing ourselves in the context of a plume acting as an interface between the ice and a quiet ocean, ocean melt has been shown to depend on ice slope [*Jenkins*, 1991b]. This connection results from two concurrent gravitational effects. Melt injects buoyancy in the plume but also tends to stratify the water column. Thus, a steeper slope increases the gravitational driving force of the plume but also decreases the stability of the stratification. Both effects act in concert to entrain warmer ambient fluid in the plume and increase melt.

Under PIG, ocean flows of $0.1\,\mathrm{m\,s^{-1}}$ appear directed along channels, and the water column is stratified within a meter of the ice base [*Stanton et al.*, 2013]. The notion of a well-mixed plume adjoining the ice base might therefore not be directly applicable. Furthermore, in such a setting, and at the terrace scale, it is unclear that the terrace walls, sloping in a direction perpendicular to the flow (i.e., transverse to the main channel axis), have a significant impact on the channel-scale buoyancy-driven acceleration, associated entrainment, and melt. Instead, we propose that on terraces, stratification limits the upward diapycnal heat flux. On the terrace walls, the oceanic heat reservoir is more readily accessible via lateral turbulent diffusion, accentuating existing wall slopes and evolving the complex coupled ice-ocean system that we observe.

6. Conclusion

Beyond the apparent complexity of the shape of the underside of ice shelves, our observations show the presence of simpler, well-defined features, namely, basal terraces where oceanic melting is subdued. These terraces are widespread and prevalent on two ice shelves from different environments and thus might be common ice shelf features.

In whichever way they are originally formed, and because of the more efficient horizontal heat transport toward the wall, far from smoothing out the features, melting is instrumental in maintaining or even creating them. While the impact of such features on the overall ice shelf mass balance remains unclear, this highlights an intricate but fundamental coupling between ocean stratification, basal melting, and ice geometry. This also warrants further attention be paid to glacial, oceanic, and coupled processes at fine spatial scales. Models might need to properly incorporate fine-scale effects, and point measurements of melt need to be placed within a detailed geometric and oceanographic context.

Acknowledgments

P.D. was supported by the NERC grants NE/G001367/1 and NE/J005770/1. Stanley S. Jacobs and NSF are acknowledged for providing shipboard support during the Autosub observations. Stephen D. McPhail, James R. Perrett, Andrew T. Webb, and David White are acknowledged for configuring and preparing the Autosub missions. Field work on Petermann glacier was supported by the NSF grant NAG5-12075 and a NASA grant from the Cryopshere Science Program. The data used to produce the results of this paper are freely available upon request to the authors.

The Editor thanks anonymous reviewers for their assistance in evaluating this paper.

References

Bindschadler, R., D. G. Vaughan, and P. Vornberger (2011), Variability of basal melt beneath the Pine Island Glacier ice shelf, West Antarctica, *J. Glaciol.*, *57*(204), 581–595, doi:10.3189/002214311797409802.

Corr, H. F. J., A. Jenkins, K. W. Nicholls, and C. S. M. Doake (2002), Precise measurement of changes in ice-shelf thickness by phase-sensitive radar to determine basal melt rates, *Geophys. Res. Lett.*, *29*(8), 1232, doi:10.1029/2001GL014618.

De Angelis, H., and P. Skvarca (2003), Glacier surge after ice shelf collapse, *Science*, *299*(5612), 1560–2, doi:10.1126/science.1077987.

Depoorter, M. A., J. L. Bamber, J. A. Griggs, J. T. M. Lenaerts, S. R. M. Ligtenberg, M. R. van den Broeke, and G. Moholdt (2013), Calving fluxes and basal melt rates of Antarctic ice shelves, *Nature*, 1–5, doi:10.1038/nature12567.

De Rydt, J., P. R. Holland, P. Dutrieux, and A. Jenkins (2014), Geometric and oceanographic controls on melting beneath Pine Island Glacier, *J. Geophys. Res. Oceans*, *119*, 2420–2438, doi:10.1002/2013JC009513.

Dutrieux, P., D. G. Vaughan, H. F. J. Corr, A. Jenkins, P. R. Holland, I. Joughin, and A. H. Fleming (2013), Pine Island glacier ice shelf melt distributed at kilometre scales, *Cryosphere*, *7*(5), 1543–1555, doi:10.5194/tc-7-1543-2013.

Dutrieux, P., J. De Rydt, A. Jenkins, P. R. Holland, H. K. Ha, S. H. Lee, E. J. Steig, Q. Ding, E. P. Abrahamsen, and M. Schröder (2014), Strong sensitivity of pine island ice-shelf melting to climatic variability, *Science*, *3*(7), 468–472, doi:10.1126/science.1244341.

Favier, L., G. Durand, S. L. Cornford, G. H. Gudmundsson, O. Gagliardini, F. Gillet-Chaulet, T. Zwinger, A. J. Payne, and A. M. Le Brocq (2014), Retreat of Pine Island Glacier controlled by marine ice-sheet instability, *Nat. Clim. Change*, *4*(2), 117–121, doi:10.1038/nclimate2094.

Gladish, C. V., D. M. Holland, P. R. Holland, and S. F. Price (2012), Ice-shelf basal channels in a coupled ice/ocean model, *J. Glaciol.*, *58*(212), 1227–1244, doi:10.3189/2012JoG12J003.

Holland, P. R., A. Jenkins, and D. M. Holland (2008), The response of ice shelf basal melting to variations in ocean temperature, *J. Clim.*, *21*(11), 2558–2572, doi:10.1175/2007JCLI1909.1.

Huppert, H. E., and J. S. Turner (1978), On melting icebergs, *Nature*, *271*(5640), 46–48, doi:10.1038/271046a0.

Jacobs, S. S., H. E. Huppert, G. Holdsworth, and D. J. Drewry (1981), Thermohaline steps induced by melting of the Erebus Glacier Tongue, *J. Geophys. Res.*, *86*(C7), 6547, doi:10.1029/JC086iC07p06547.

Jacobs, S. S., A. Jenkins, C. F. Giulivi, and P. Dutrieux (2011), Stronger ocean circulation and increased melting under Pine Island Glacier ice shelf, *Nat. Geosci.*, *4*(8), 519–523, doi:10.1038/ngeo1188.

Jenkins, A. (1991a), A one-dimensional model of ice shelf-ocean interaction, *J. Geophys. Res.*, *96*(C11), 20,671, doi:10.1029/91JC01842.

Jenkins, A. (1991b), Gravity currents beneath ice shelves, in *Glacier-Ocean-Atmosphere Interactions*, edited by V. M. Kotlyakov, A. Ushakov, and A. Glazovsky, pp. 177–182, IAHS, St Petersburg / Leningrad, Russia.

Jenkins, A., H. F. J. Corr, K. W. Nicholls, C. L. Stewart, and C. S. M. Doake (2006), Interactions between ice and ocean observed with phase-sensitive radar near an Antarctic ice-shelf grounding line, *J. Glaciol.*, *52*(178), 325–346, doi:10.3189/172756506781828502.

Jenkins, A., P. Dutrieux, S. S. Jacobs, S. D. McPhail, J. R. Perrett, A. T. Webb, and D. White (2010), Observations beneath Pine Island glacier in West Antarctica and implications for its retreat, *Nat. Geosci.*, *3*(7), 468–472, doi:10.1038/ngeo890.

Johnson, H. L., A. Münchow, K. K. Falkner, and H. Melling (2011), Ocean circulation and properties in Petermann Fjord, Greenland, *J. Geophys. Res.*, *116*, C01003, doi:10.1029/2010JC006519.

Joughin, I., B. E. Smith, and D. M. Holland (2010), Sensitivity of 21st century sea level to ocean-induced thinning of Pine Island Glacier, Antarctica, *Geophys. Res. Lett.*, *37*, L20502, doi:10.1029/2010GL044819.

Korona, J., E. Berthier, M. Bernard, F. Rémy, and E. Thouvenot (2009), SPIRIT. SPOT 5 stereoscopic survey of Polar Ice: Reference Images and Topographies during the fourth International Polar Year (2007–2009), *ISPRS J. Photogramm. Remote Sens.*, *64*(2), 204–212, doi:10.1016/j.isprsjprs.2008.10.005.

Le Brocq, A. M., et al. (2013), Evidence from ice shelves for channelized meltwater flow beneath the Antarctic Ice Sheet, *Nat. Geosci.*, *6*(11), 945–948, doi:10.1038/ngeo1977.

Millgate, T., P. R. Holland, A. Jenkins, and H. L. Johnson (2013), The effect of basal channels on oceanic ice-shelf melting, *J. Geophys. Res. Oceans*, *118*, 6951–6964, doi:10.1002/2013JC009402.

Mölg, T. (2003), Solar-radiation-maintained glacier recession on Kilimanjaro drawn from combined ice-radiation geometry modeling, *J. Geophys. Res.*, *108*(D23), 4731, doi:10.1029/2003JD003546.

Moon, T., I. Joughin, B. Smith, and I. Howat (2012), 21st-century evolution of Greenland outlet glacier velocities, *Science*, *336*(6081), 576–8, doi:10.1126/science.1219985.

Mouginot, J., E. Rignot, and B. Scheuchl (2014), Sustained increase in ice discharge from the Amundsen Sea Embayment, West Antarctica, from 1973 to 2013, *Geophys. Res. Lett.*, *41*, 1576–1584, doi:10.1002/2013GL059069.

Nicholls, K. W., et al. (2006), Measurements beneath an Antarctic ice shelf using an autonomous underwater vehicle, *Geophys. Res. Lett.*, *33*, L08612, doi:10.1029/2006GL025998.

Park, J. W., N. Gourmelen, A. Shepherd, S. W. Kim, D. G. Vaughan, and D. J. Wingham (2013), Sustained retreat of the Pine Island Glacier, *Geophys. Res. Lett.*, *40*, 2137–2142, doi:10.1002/grl.50379.

Post, A., and E. R. LaChapelle (1999), *Glacier Ice*, Revised ed., University of Washington Press and International Glaciological Society, Cambridge, U. K.

Pritchard, H. D., S. R. M. Ligtenberg, H. A. Fricker, D. G. Vaughan, M. R. van den Broeke, and L. Padman (2012), Antarctic ice-sheet loss driven by basal melting of ice shelves, *Nature*, *484*(7395), 502–5, doi:10.1038/nature10968.

Rignot, E., and K. Steffen (2008), Channelized bottom melting and stability of floating ice shelves, *Geophys. Res. Lett.*, *35*, L02503, doi:10.1029/2007GL031765.

Rignot, E., S. Jacobs, J. Mouginot, and B. Scheuchl (2013), Ice-shelf melting around Antarctica, *Science*, *341*(6143), 266–70, doi:10.1126/science.1235798.

Sergienko, O. V. (2013), Basal channels on ice shelves, *J. Geophys. Res. Earth Surf.*, *118*, 1342–1355, doi:10.1002/jgrf.20105.
Shepherd, A., D. Wingham, and E. Rignot (2004), Warm ocean is eroding West Antarctic Ice Sheet, *Geophys. Res. Lett.*, *31*, L23402, doi:10.1029/2004GL021106.
Shepherd, A., et al. (2012), A reconciled estimate of ice-sheet mass balance, *Science*, *338*(6111), 1183–9, doi:10.1126/science.1228102.
Stanton, T. P., W. J. Shaw, M. Truffer, H. F. J. Corr, L. E. Peters, K. L. Riverman, R. Bindschadler, D. M. Holland, and S. Anandakrishnan (2013), Channelized ice melting in the ocean boundary layer beneath Pine Island Glacier, Antarctica, *Science*, *341*(6151), 1236–9, doi:10.1126/science.1239373.
Straneo, F., D. A. Sutherland, D. Holland, C. Gladish, G. S. Hamilton, H. L. Johnson, E. Rignot, Y. Xu, and M. Koppes (2012), Characteristics of ocean waters reaching Greenland's glaciers, *Ann. Glaciol.*, *53*(60), 202–210, doi:10.3189/2012AoG60A059.
Thurnherr, A. M., S. S. Jacobs, P. Dutrieux, and C. F. Giulivi (2014), Export and circulation of ice cavity water in Pine Island Bay, West Antarctica, *J. Geophys. Res. Oceans*, *119*, 1754–1764, doi:10.1002/2013JC009307.
Vaughan, D. G., H. F. J. Corr, R. Bindschadler, P. Dutrieux, G. H. Gudmundsson, A. Jenkins, T. Newman, P. Vornberger, and D. J. Wingham (2012), Subglacial melt channels and fracture in the floating part of Pine Island Glacier, Antarctica, *J. Geophys. Res.*, *117*, F03012, doi:10.1029/2012JF002360.
Whitworth, T., A. H. Orsi, S.-J. Kim, W. D. Nowlin, and R. A. Locarnini (1998), Water masses and mixing near the Antarctic slope front, in *Ocean, Ice, and Atmosphere: Interactions at the Antarctic Continental Margin*, *Antarct. Res. Ser.*, vol. 75, edited by S. S. Jacobs and R. F. Weiss, pp. 1–28, AGU, Washington, D. C.